

Prompt neutrino fluxes from atmospheric charm

Rikard Enberg,¹ Mary Hall Reno,² and Ina Sarcevic¹

¹*Department of Physics, University of Arizona, Tucson, AZ 85721*

²*Department of Physics and Astronomy, University of Iowa, Iowa City, IA*

We calculate the prompt neutrino flux from atmospheric charm production by cosmic rays, using the dipole picture in a perturbative QCD framework, which incorporates the parton saturation effects present at high energies. We compare our results with the next-to-leading order perturbative QCD result and find that saturation effects are large for neutrino energies above 10^6 GeV, leading to a substantial suppression of the prompt neutrino flux. We comment on the range of prompt neutrino fluxes due to theoretical uncertainties.

I. INTRODUCTION

Atmospheric neutrinos are produced in interactions of cosmic rays with Earth's atmosphere. The observation of low energy ($E_\nu \sim \text{GeV}$) atmospheric neutrinos, their flavor-dependent interactions, and their path length dependence [1, 2] has confirmed the existence of neutrino flavor transformation, and therefore the most fundamental property of the neutrinos: that they are not massless. These observations have provided a remarkable source of information about mass and mixing parameters of neutrinos.

Atmospheric neutrinos are also a background to other sources of neutrinos, such as cosmogenic neutrinos produced in interactions of cosmic rays with the background radiation [3] and directly from sources such as active galactic nuclei and gamma ray bursts [4]. Observation of neutrinos coming from these distant sources would provide valuable information about the particle production mechanism in astrophysical sources.

Neutrino interactions in the Earth and in the atmosphere could also serve as unique probes of physics beyond the Standard Model [5]. It has been recently suggested that atmospheric neutrinos, in their interactions in the Earth, could produce supersymmetric particles if the neutrino energies are sufficiently high. In Ref. [6], Ando et al. have suggested that the high energy atmospheric neutrino flux may be large enough to produce quasi-stable charged particles that are potentially detectable in the IceCube [7] neutrino detector. As a background to high energy sources or as a flux to produce exotic particles in the Earth, it is useful to re-evaluate the high energy component of the atmospheric neutrino flux.

The atmospheric fluxes of neutrinos at low energies have been extensively studied [8, 9, 10, 11]. They arise mainly from the products of charged pion and kaon decays. As energies increase, the decay lengths of the mesons become longer than their path lengths in the atmosphere [12], suppressing the production of neutrinos. Other, shorter lived hadrons are also produced at high energies. They too contribute to the neutrino flux, especially from the “prompt” decay of charmed mesons. The energy dependence of these prompt neutrinos is less steep than the “conventional” neutrino flux from pion and kaon decays. The energy at which the

prompt neutrinos become the dominant atmospheric neutrino component depends on the details of the mechanism for charm production in proton–air collisions at high energies. Charm contributions to the atmospheric lepton fluxes have been evaluated analytically and semi-analytically [13, 14, 15, 16, 17]. There are renewed efforts include charm production with the dual parton model in Monte Carlo simulations of air showers as well [18, 19].

For vertical neutrino fluxes, the cross-over between conventional and prompt dominated fluxes occurs in the energy range of 10^5 – 10^6 GeV for the calculations of Refs. [14, 15, 16, 17], and the cross-over energy increases with zenith angle. For energies above $\sim 10^6$ GeV, the dominant contribution to charm production comes from gluons, where saturation effects [20] due to dense, interacting gluons in the nucleus become important. We evaluate the prompt neutrino flux using perturbative QCD in the dipole framework, taking these effects into account. We study the theoretical uncertainties inherent in this approach and compare with standard next-to-leading order perturbative QCD. The range of QCD-based predictions yields prompt neutrino fluxes that are unlikely to be large enough to produce a detectable number of exotic particles of the type discussed in Ref. [6].

We begin with a discussion of the cross section for charm production in the dipole picture in Section II. Using the dipole picture results, we discuss the evaluation of the prompt neutrino flux from charm decays in Section III. Our results and a comparison with the conventional fluxes are shown in Section IV. We also discuss uncertainties in the QCD approach, and compare our results with the uncertainty band of Ref. [6] in Section IV.

II. CROSS SECTION FOR CHARM PRODUCTION

A. Charm production in perturbative QCD

In the perturbative QCD approach, the dominant contribution to the charm cross section at high energies comes from the partonic subprocess $gg \rightarrow c\bar{c}$. The parton-level differential cross section for production of $c\bar{c}$ pairs in proton–proton collision, at the leading order

in the strong coupling constant, $\alpha_s(\mu^2)$, is given by

$$\frac{d\sigma_{\text{LO}}}{dx_F} = \int \frac{dM_{c\bar{c}}^2}{(x_1 + x_2)s} \sigma_{gg \rightarrow c\bar{c}}(\hat{s}) G(x_1, \mu^2) G(x_2, \mu^2) \quad (1)$$

where $x_{1,2}$ are the momentum fractions of the gluons, $x_F = x_1 - x_2$ is the Feynman variable, $G(x, \mu^2)$ is the gluon distribution of the proton, and μ is the factorization scale. Given the charm–anticharm invariant mass $M_{c\bar{c}}$, the fractional momenta of the gluons, $x_{1,2}$, can be expressed in terms of the the Feynman variable, x_F ,

$$x_{1,2} = \frac{1}{2} \left(\sqrt{x_F^2 + \frac{4M_{c\bar{c}}^2}{s}} \pm x_F \right). \quad (2)$$

Typically the factorization scale is taken to be of the order of $2m_c$.

For the flux calculation we need the differential cross section as a function of incident proton energy (E_p) and final charm energy (E_c), convoluted with the incident cosmic ray proton flux. Clearly at high energies, given the relationship of Eq. (2), the charm cross section has dominant contribution when one gluon parton distribution function (PDF) is at $x_1 \sim x_F$ and the other gluon distribution is at $x_2 \ll 1$. Since the gluon distribution cannot be measured directly, its value at very small x has large uncertainties, especially for the low factorization scale $\mu \sim 2m_c$. The dipole picture gives a theoretically motivated description of small x physics which can effectively take into account resummation of the large $\alpha_s \ln(1/x)$ contributions [21] to the evolution of the PDFs. Thus by using the dipole picture, we avoid the large uncertainty due to the unknown behavior of the gluon distribution at very small x .

The dipole picture is most straightforwardly described in the DIS context, which we do next. We then elaborate how this is applied to hadron–hadron scattering.

B. Dipole picture formalism in deep inelastic scattering

In deep inelastic lepton–hadron scattering, the high Q^2 virtual photon can penetrate the nucleon and probe the partonic degrees of freedom. This partonic interpretation based on perturbative QCD is most relevant in the infinite momentum frame. The Q^2 -dependence of the nucleon structure function $F_2^N(x, Q^2)$ is well accounted for by the DGLAP evolution equations [22] given some non-perturbative initial condition $F_2^N(x, Q_0^2)$. As noted above, at small x one needs to consider the resummation of large logarithms $\ln 1/x$, which leads to the BFKL evolution equation [21].

Another feature of the nucleon structure function F_2^N in the DGLAP framework is the strong growth of the gluon density in the nucleon in the small x region. In the infinite momentum frame, because of the high nucleon and parton densities, quarks and gluons that belong to different nucleons in the nucleus may recombine

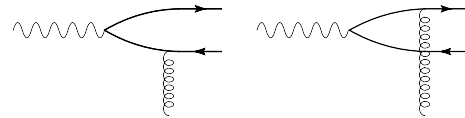


FIG. 1: The perturbative diagrams giving rise to scattering with a gluon of the $\gamma^* \rightarrow q\bar{q}$ fluctuation in deep inelastic scattering.

and annihilate, leading to the recombination effect first proposed by Gribov, Levin and Ryskin (GLR) [20] and later detailed by Mueller and Qiu [23].

An alternative approach is to consider instead the interaction in the target rest frame (laboratory frame), where the virtual photon interacts with nucleons via its quark–antiquark pair ($q\bar{q}$) color-singlet fluctuation [24]. If the coherence length of the virtual photon fluctuation is larger than the radius of the nucleus, $l_c > R_A$, the $q\bar{q}$ configuration interacts coherently with all nucleons, with a cross section given by the color transparency mechanism for a pointlike color-singlet configuration [25]. That is, the cross section is proportional to the transverse separation squared, r^2 , of the q and \bar{q} .

In the dipole picture, the cross section for the absorption of a virtual photon in the small x region is dominated by the scattering of a gluon off the $q\bar{q}$ pair fluctuation of the virtual photon. The generic perturbative QCD diagrams giving rise to the $q\bar{q}$ fluctuation are shown in Figure 1. The invariant mass of the incoming virtual photon-proton system at small x is related to the photon virtuality Q^2 by

$$s = (q + p)^2 \simeq 2p \cdot q = \frac{Q^2}{x}, \quad (3)$$

where q and p are the four-momenta of the photon and the target nucleon, $q^2 = -Q^2$ and $x = Q^2/2p \cdot q$. Thus the region of small x corresponds to a high energy scattering process at fixed Q^2 .

The imaginary part of the sum of the amplitudes in Figure 1 is related to the photoabsorption cross section, which has been calculated by Nikolaev and Zakharov [26] assuming that the size of the $q\bar{q}$ pair is frozen in the scattering process and that the one-gluon exchange process of Figure 1 dominates. The transverse cross section can be cast into an impact parameter representation

$$\sigma(\gamma^* N) = \int_0^1 dz \int d^2\mathbf{r} |\Psi_T(z, \mathbf{r}, Q^2)|^2 \sigma_{q\bar{q}N}(x, \mathbf{r}), \quad (4)$$

where z is the Sudakov variable, defined to be the fraction of the $q\bar{q}$ pair momentum carried by the quark, and \mathbf{r} is the variable conjugate to the transverse momentum of the quark, representing the transverse size of the pair. The function $\Psi_T(z, \mathbf{r}, Q^2)$ can be interpreted as the wave function of the $q\bar{q}$ fluctuations of the virtual photon. Thus, $|\Psi_T(z, \mathbf{r}, Q^2)|^2$ is the probability of finding a $q\bar{q}$ pair with a separation \mathbf{r} and a fractional momentum z . It is given

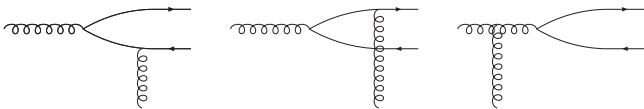


FIG. 2: The perturbative diagrams giving rise to the scattering of a gluon with the $g \rightarrow q\bar{q}$ pair fluctuation in hadronic collisions.

for each quark flavor f with fractional charge e_f by [26]

$$|\Psi_T^f(z, \mathbf{r}, Q^2)|^2 = \quad (5)$$

$$e_f^2 \frac{\alpha_{em} N_c}{2\pi^2} [(z^2 + (1-z)^2) \epsilon^2 K_1^2(\epsilon r) + m_f^2 K_0^2(\epsilon r)],$$

where $\epsilon^2 = z(1-z)Q^2 + m_f^2$, and K_0 and K_1 are modified Bessel functions.

The cross section for the high energy interaction of a small-size $q\bar{q}$ configuration with the nucleon, $\sigma_{q\bar{q}N}(\mathbf{r})$, can be calculated in leading-order perturbative QCD. In this approximation, one sets $\sigma_{q\bar{q}N}(\mathbf{r})$ equal to [27]

$$\sigma_d^{pQCD} = \frac{\pi^3}{3} r^2 \alpha_s(\mu) x G(x_1, \mu^2). \quad (6)$$

This cross section is, as discussed above, proportional to the square of the size of the pointlike configuration as a consequence of color transparency in QCD. However, the singular behavior of the wave function and the strong scaling violation of the gluon distribution in the small- x region as r decreases can compensate the smallness of the cross section due to color transparency.

Ultimately, gluon saturation effects need to be included for a more realistic $\sigma_{q\bar{q}N}(\mathbf{r})$. One would then derive an approximate expression for the dipole cross section from theory, *including* saturation effects, and use experimental data to determine incalculable parameters in this expression. Before we turn to saturation and the types of functional forms used to fit the dipole cross section, in the next section we describe how heavy quark production in proton-proton scattering is treated in the dipole picture.

C. Heavy quark production

Heavy quark production in hadronic collisions can be obtained in the same formalism [28, 29, 30, 31]. In this case, the dipole is produced from a gluon instead of a photon, so that the dipole can be in a color octet state. As shown in Figure 2, there is now an additional diagram that contributes, in which the gluon interacts with the target before fluctuating to a dipole.

The differential cross section for heavy quark production is [28]

$$\frac{d\sigma(pp \rightarrow Q\bar{Q}X)}{dy} \simeq x_1 G(x_1, \mu^2) \sigma^{Gp \rightarrow Q\bar{Q}X}(x_2, \mu^2, Q^2), \quad (7)$$

where x_1 and x_2 are the partonic momentum fractions, $y = \frac{1}{2} \ln(x_1/x_2)$ is the $Q\bar{Q}$ pair rapidity and $\sigma^{Gp \rightarrow Q\bar{Q}X}$ is the partonic cross section calculated in the dipole model,

$$\sigma^{Gp \rightarrow Q\bar{Q}X}(x, \mu^2, Q^2) = \int dz d^2\mathbf{r} |\Psi_G^Q(z, \mathbf{r})|^2 \sigma_{dG}(x, \mathbf{r}). \quad (8)$$

The probability of finding a $Q\bar{Q}$ pair with a separation \mathbf{r} and a fractional momentum z , is given by

$$|\Psi_G^Q(z, \mathbf{r}, Q^2 = 0)|^2 = \quad (9)$$

$$\frac{\alpha_s(\mu)}{2\pi^2} [(z^2 + (1-z)^2) m_Q^2 K_1^2(m_Q r) + m_Q^2 K_0^2(m_Q r)],$$

where $\mu \sim 1/r$ is the factorization scale. For heavy quark production we have $Q^2 = 0$, so $\mu \sim m_Q$ and $\epsilon = m_Q$.

The dipole cross section that describes the interaction of a heavy quark–antiquark pair from the fluctuation of a gluon with the target nucleon is given by [28]

$$\sigma_{GQ\bar{Q}}^N(x_2, \mathbf{r}) = \frac{9}{8} [\sigma_d(x_2, z\mathbf{r}) + \sigma_d(x_2, (1-z)\mathbf{r})] - \frac{1}{8} \sigma_d(x_2, \mathbf{r}), \quad (10)$$

where σ_d is the color singlet dipole cross section of Eq. (4). The first term corresponds to the quark–gluon ($G-Q$) separation $z\mathbf{r}$, the antiquark–gluon ($G-\bar{Q}$) separation $(1-z)\mathbf{r}$ and the quark–antiquark ($Q-\bar{Q}$) separation \mathbf{r} . This expression includes contributions from the three different color and spin states in which $Q\bar{Q}$ can be produced [30].

Finally, to take threshold corrections for charm production at large x into account, the dipole cross section is multiplied with a factor $(1-x_2)^7$ [32]. We find this correction to be negligible for energies above 10^3 GeV.

D. The dipole–proton cross section and saturation

The dynamics of the scattering process at small x is, in principle, included in the dipole cross section. Thus, to compute the differential cross section $d\sigma/dx_F$ we must find the cross section for a $c\bar{c}$ dipole to scatter on the proton, including the effects of saturation.

A simple model for saturation was proposed by Golec-Biernat and Wüsthoff [33]. In their model, the dipole cross section is parametrized as

$$\sigma_d^{GBW} = \sigma_0 [1 - e^{-r^2 Q_s^2(x)/4}], \quad (11)$$

where Q_s is the saturation scale,

$$Q_s = Q_s(x) = Q_0(x_0/x)^{\lambda/2} \quad (12)$$

with $Q_0 = 1$ GeV. The parameters λ and x_0 in the above expressions were fitted to HERA data on the structure function F_2 and the diffractive structure function F_2^D [33].

This is a phenomenological model, constructed to give the right behavior of the dipole cross section in the two limits $r \rightarrow 0$ and $r \rightarrow \infty$. Eq. (11) has $\sigma \propto r^2$ for small r , as implied by perturbative QCD, and $\sigma \rightarrow \text{const}$ for large r (this is the saturation property of the cross section), thus providing some insight into the physics of saturation. The simple parametrization also gave a good fit to the data, although it does not reproduce newer data as well [34] as it does the older data.

One would like to calculate the dipole cross section rigorously in perturbative QCD; however, it is not known how to fully include the effects of saturation. It is convenient to study QCD evolution in Mueller’s dipole formulation [35], where the projectile contains a collection of color dipoles. It has been shown [36] that in the high-energy limit, the scattering process is equivalent to a stochastic reaction–diffusion process where there are fluctuations in the number of dipoles. These fluctuations may potentially have a large effect on the energy dependence of the amplitude and saturation scale. A full calculation should include these effects, but they were found to be small in the region of very small x [37]. In principle one should also take into account the complicated dynamics of the color glass condensate [38, 39, 40, 41]. This is described by the functional integro-differential Jalilian-Marian, Iancu, McLerran, Weigert, Leonidov and Kovner (JIMWLK) equations [39], or equivalently by Balitsky’s infinite hierarchy of coupled differential equations for the expectation values of Wilson lines [40].

A much simpler equation which includes saturation was obtained by Balitsky [40] and Kovchegov [42] in the particular case where the target is a large nucleus. This equation is known as the Balitsky–Kovchegov (BK) equation and although it can be derived within the dipole framework, it turns out to represent a specific mean-field approximation to the Balitsky–JIMWLK equations. The BK equation is, like the BFKL equation, a leading logarithmic evolution equation in $\ln(1/x)$. The BFKL equation, however, is a linear equation, while the BK equation is similar in structure to the GLR [20] and Muller–Qiu [23] equations, and can be written as the BFKL equation modified by a non-linear term. This reduces the power growth of the gluon distribution as $x \rightarrow 0$, which has been established by both numerical and approximate analytical studies, see e.g. Ref. [37] and references therein.

The dipole cross section is obtained from the solution of the BK equation, which can be solved numerically. We will instead use an approximate result [43], which consists of a matching of approximate analytic solutions of the BK equation in the two regions of dipole size $r \gg 1/Q_s$ and $r \ll 1/Q_s$, where the equation simplifies.

In the large r region the solution approaches a fixed saturated value as $r \rightarrow \infty$ [44]. For $r \ll 1/Q_s$ the effects of the non-linearity in the BK equation are small, and the equation reduces to the BFKL equation; the solution is a saddle point solution of the BFKL equation, subject to a saturation condition [43]. The two solutions are matched

Ref.	\mathcal{N}_0	γ_s	λ	x_0	σ_0 (mb)
[43]	0.7	0.627	0.253	0.267×10^{-4}	25.8
[45]	0.7	0.627	0.175	0.19×10^{-6}	37.3
[46]	0.7	0.738	0.220	0.163×10^{-4}	27.3

TABLE I: Parameter values in the dipole cross section formulas in Eqs. (13) and (14). In Refs. [43] and [45], γ_s is calculated, while in Ref. [46], it is a fit parameter.

at an intermediate scale $rQ_s = 2$. The resulting model is what we will refer to as the dipole model (DM).

The dipole cross section is given by

$$\sigma_d(x, \mathbf{r}) = \sigma_0 \mathcal{N}(rQ_s, Y), \quad (13)$$

where σ_0 is a constant, and \mathcal{N} is the forward dipole scattering amplitude obtained from the BFKL or BK equation [43],

$$\mathcal{N}(rQ_s, Y) = \begin{cases} \mathcal{N}_0 \left(\frac{\tau}{2}\right)^{2\gamma_{\text{eff}}(x,r)}, & \text{for } \tau < 2 \\ 1 - \exp[-a \ln^2(b\tau)], & \text{for } \tau > 2. \end{cases} \quad (14)$$

Here $\tau = rQ_s$, $Y = \ln(1/x)$ is the rapidity, and again the saturation scale is defined in Eq. (12) with $Q_0 = 1$ GeV. Furthermore,

$$\gamma_{\text{eff}}(x, r) = \gamma_s + \frac{\ln(2/\tau)}{\kappa \lambda Y} \quad (15)$$

is the “effective anomalous dimension,” and γ_s and κ are theoretical parameters calculated from the BFKL equation, with numerical values $\gamma_s = 0.627$ and $\kappa = 9.94$. Note that this is a perturbative QCD result and not an *ad hoc* model, although it is obtained by an approximate solution of the BK equation.

The free parameters in the model are \mathcal{N}_0 , σ_0 , λ and x_0 . In Ref. [43], the first of these was chosen to take the value 0.7. The exponent λ specifies the power behavior of the saturation scale with x , and x_0 is the value of x where the saturation scale is 1 GeV. Furthermore, a and b are matching coefficients to be chosen such that the dipole amplitude and its derivative with respect to r are continuous at $\tau = 2$. We find

$$a = -\frac{\ln(1 - \mathcal{N}_0)}{\ln^2(1 - \mathcal{N}_0)^{\frac{1}{\gamma_s} - \frac{1}{\mathcal{N}_0\gamma_s}}} \quad (16)$$

$$b = \frac{1}{2}(1 - \mathcal{N}_0)^{\frac{1}{\gamma_s} - \frac{1}{\mathcal{N}_0\gamma_s}}. \quad (17)$$

Note that the amplitude is a function of r and x only in the combination indicated, $\tau \equiv rQ_s(x)$, except for the geometric scaling breaking term in the effective anomalous dimension which contains the rapidity.

The fitted parameter values from three different fits to HERA data on the deep inelastic structure function F_2 at small x [43, 45, 46] are shown in Table I. Note

that in all cases \mathcal{N}_0 was fixed at $\mathcal{N}_0 = 0.7$. The first row shows the original parameter values obtained in Ref. [43]. This was a three-flavor fit and is therefore not suitable for our calculation, but it has been extended to include charm [45], giving the values in the second row. Finally, the third row shows a more recent fit by Soyez [46], which also includes charm. In this fit the parameter γ_s was taken as a free parameter, which gave a better fit to the data, with a larger value of γ_s and a smaller value of λ . This is quite interesting since a reduction of these parameters is exactly what is expected when including higher order logarithmic corrections to the BFKL kernel in the BK equation [47].

These models take into account only the leading exponential x -dependence of the saturation scale, and there are large sub-asymptotic corrections to the energy dependence [48],

$$\ln Q_s^2(Y) = \frac{3\alpha_s}{\pi} \frac{\chi(\gamma_s)}{\gamma_s} Y - \frac{3}{2\gamma_s} \ln Y - \frac{3}{\gamma_s^2} \sqrt{\frac{2\pi}{\bar{\alpha}\chi''(\gamma_s)}} \frac{1}{\sqrt{Y}} + \mathcal{O}(1/Y), \quad (18)$$

where $\chi(\gamma)$ is the BFKL characteristic function and $\gamma_s = 0.627$. The models discussed in this section keep only the leading term in this expression. Using the full expression could potentially change the energy dependence of the cross section substantially, but to incorporate this in this dipole model would require introducing more parameters and performing a new fit to all the data.

In the dipole model results that follow, the DM results shown use the parameters of Soyez [46] shown in Table I and the parametrization of equations (13–14).

E. Nuclear effects

In a dipole framework there are two possible ways to include nuclear effects suggested in the literature: modification of the saturation scale, e.g. as proposed by Armesto, Salgado and Wiedemann (ASW) [49] (see also [50] for another approach), and the Glauber–Gribov [51, 52] formalism. In the former case, the nuclear effects are accounted for by geometric scaling, simply scaling the saturation scale for a nucleus A according to

$$Q_{s,A}^2 = Q_{s,p}^2 \left(\frac{A\pi R_p^2}{\pi R_A^2} \right)^{1/\delta} \quad (19)$$

where R_p is the proton radius, $R_A = 1.12A^{1/3} - 0.86A^{-1/3}$ fm is the nuclear radius, and δ is a free parameter to be fitted to data. ASW find $\delta = 0.79$ by fitting to γ^*A data at small x . The proton radius is related to σ_0 in the dipole cross section through $\sigma_0 = 2\pi R_p^2$.

In the Glauber–Gribov formalism, nuclear rescattering is taken into account by integrating the dipole cross

section for dipole–nucleus collisions over the impact parameter,

$$\sigma_d^A(x, r) = \int d^2b \sigma_d^A(x, r, b), \quad (20)$$

where b is the impact parameter between the center of the dipole and the center of the nucleus. The expression for the b -dependent cross section is given by

$$\sigma_d^A(x, r, b) = 2 \left[1 - \exp \left(-\frac{1}{2} A T_A(b) \sigma_d^p(x, r) \right) \right], \quad (21)$$

where $\sigma_d^p(x, r)$ is the dipole–proton cross section given in Eqs. (13) and (14) and $T_A(b)$ is the nuclear profile function,

$$T_A(b) = \int dz \rho_A(z, \mathbf{b}), \quad (22)$$

where ρ_A is the nuclear density, and T_A is normalized so that

$$\int d^2b T_A(b) = 1. \quad (23)$$

This model has e.g. been used in Ref. [53] with a Fermi distribution for ρ to compute nuclear structure functions with good results.

We compared the Glauber–Gribov model with a Gaussian distribution for ρ to the ASW method and found that for the relatively light air nuclei, these two methods give very similar results (within 10%). We will in the following use the simpler ASW method.

Predictions from the framework described above have been tested against data. For deep inelastic structure functions this was done in Refs. [43, 46]. The ratio of DIS on nuclei to DIS on deuterons was calculated and compared to E665 data in Ref. [54], and total cross sections for γp , γA , pp , and pA were calculated in [31] using the parameters from [45] (second row in Table I), and the γp and pp results were compared to data with good agreement. There have been no tests in the energy range probed by cosmic rays. However, the LHC will begin to access these energy scales shortly.

F. Fragmentation of charm quarks

Our earlier analytical calculation [14] did not take fragmentation of the charm quarks into charmed hadrons into account, but simply took the hadron to have the same energy as the charm quark. In Ref. [16], fragmentation was taken into account by decreasing the momentum fraction of the hadron to an average lower value. In this paper we take fragmentation into account by using fragmentation functions.

For our comparison without fragmentation, we use updated hadron fractions [55]

$$f_{D^0} = 0.565, \quad f_{D^+} = 0.246, \quad f_{D_s^+} = 0.080, \quad f_{\Lambda_c} = 0.094 \quad (24)$$

Hadron h	N_h	ϵ_h
D^0	0.694	0.101
D^+	0.282	0.104
D_s^+	0.050	0.032
Λ_c^+	0.00677	0.00418

TABLE II: Parameters in the LO Kniehl and Kramer fragmentation model [57].

where f_h is the fraction of fragmentation of $c \rightarrow h$. These newer values are somewhat different from the values used in [14, 15, 16]; this increases the computed flux by about 20%.

In general the cross section for hadron production including fragmentation is obtained from the cross section for charm production as

$$\frac{d\sigma(pp \rightarrow hX)}{dE_h} = \int_{E_h}^{\infty} \frac{dE_c}{E_c} \frac{d\sigma(pp \rightarrow cX)}{dE_c} D_c^h(E_h/E_c), \quad (25)$$

where $D_c^h(z)$ is the fragmentation function for $c \rightarrow h$. This can be written in terms of momentum fractions as

$$\frac{d\sigma(pp \rightarrow hX)}{dx_E} = \int_{x_E}^1 \frac{dz}{z} \frac{d\sigma(pp \rightarrow cX)}{dx_c} D_c^h(z), \quad (26)$$

where $z = E_h/E_c$, $x_c = E_c/E_p$, and $x_E = E_h/E_p$. At high energy the momentum fraction $x_E \simeq x_F$, or, for the charm cross section, $x_c \simeq x_F$.

We use both the older Peterson fragmentation function [56] and the recent parametrization by Kniehl and Kramer (KK) in Ref. [57]. The Peterson function is given by

$$D_c^h(z) = N_h \frac{1}{z} \left(1 - \frac{1}{z} - \frac{\epsilon}{1-z} \right)^{-2}, \quad (27)$$

where $\epsilon = 0.05$ is a fitted parameter [55], common for all mesons, and $N_h = f_h N$ is a normalization constant where N is given by the condition

$$\sum_h \int dz D_c^h(z) = 1, \quad (28)$$

assuming that the shape of D_c^h is independent of the hadron h , and the fragmentation fractions are given in Eq. (24). The calculation without fragmentation amounts to taking fragmentation functions $D_c^h(z) = f_h \delta(1-z)$.

The KK fragmentation function has the form

$$D_c^h = N_h \frac{x(1-x)^2}{[(1-x)^2 + \epsilon_h x]^2}, \quad (29)$$

with the parameters given in Ref. [57], which we show in Table II.

The Kniehl–Kramer fragmentation functions have normalization factors fitted to the data. The integrals of

these functions give the fragmentation fractions in the KK model, and these are quite different from the values cited above: for the LO fit we obtain $f_{D^0} = 0.745$, $f_{D^+} = 0.296$, $f_{D_s^+} = 0.125$, and $f_{\Lambda_c} = 0.063$. KK also perform a NLO fit. The NLO values decreases the normalization of the calculated flux by about 10%, but as our calculation is a LO calculation it is more consistent to use the LO fit. These fragmentation fractions do not add to one, an indication of one of the theoretical uncertainties.

G. Theoretical uncertainties in the charm pair cross section

Because the charm quark mass is of order 1 GeV, there are in principle large uncertainties in the charm pair production cross section [58]. In perturbation theory using parton distribution functions, the charm cross section predictions can vary by more than an order of magnitude depending on the charm quark mass, number of flavors and choice of scales and PDFs. The dipole approach, with the fit to DIS data then translated to hadron scattering, mitigates the uncertainty. Beyond the total cross section, one is interested in the energy distribution of the charmed quark.

To investigate the sensitivity of the charm differential cross section to the choice of parameters, we vary them as follows: We use the parameters of Ref. [46] for the dipole cross section (the fit of Ref. [45] gives very similar results). We vary the PDF by taking the MRST 2001 LO [60] or the CTEQ 6L gluon distributions [61], and we vary the factorization scale between $\mu_F = 2m_c$ or $\mu_F = m_c$, where the charm quark mass is varied between $m_c = 1.3$ GeV and $m_c = 1.5$ GeV. In each of the listed cases the former choice is what we use as our “standard” curves below. In Figure 3 we show a representative set of predictions for the differential cross section $d\sigma(pA \rightarrow c\bar{c})/dx_F$ for $A = 14.5$, the average nucleon number of air, and an incident proton energy of 10^9 GeV. The parameter combinations that are not shown in the plot give results that fall between the upper and lower lines.

We are also interested in the difference between the predictions of NLO QCD and the saturation prediction of the DM model. This is illustrated in Figure 4, where we show $d\sigma(pA \rightarrow c\bar{c})/dx_F$ at three energies using these two calculations. The NLO QCD cross section come from Ref. [14] (PRS). Note that the NLO QCD cross section increases with energy much faster than the DM cross section. For the lower energy $E = 10^3$ GeV the cross sections are comparable, but we shall see that because of the different energy dependence, the neutrino flux calculated using NLO QCD is larger than the one calculated from the DM model.

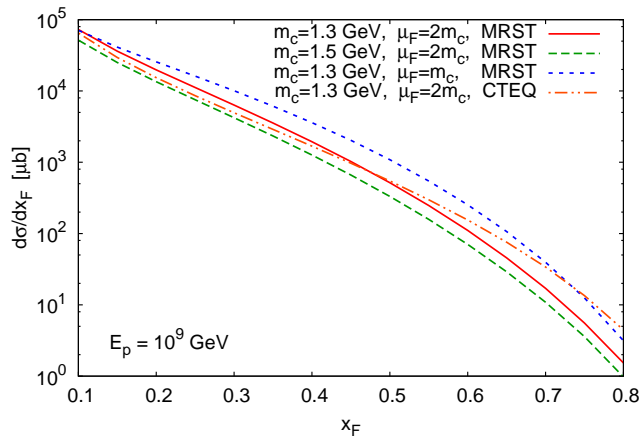


FIG. 3: Charm quark x_F distribution in proton-air collisions at $E_p = 10^9$ GeV, calculated in the dipole model described in the text, with the “standard” choices of $m_c = 1.3$ GeV, factorization scale $\mu_F = 2m_c$ and the MRST2001 PDFs [60].

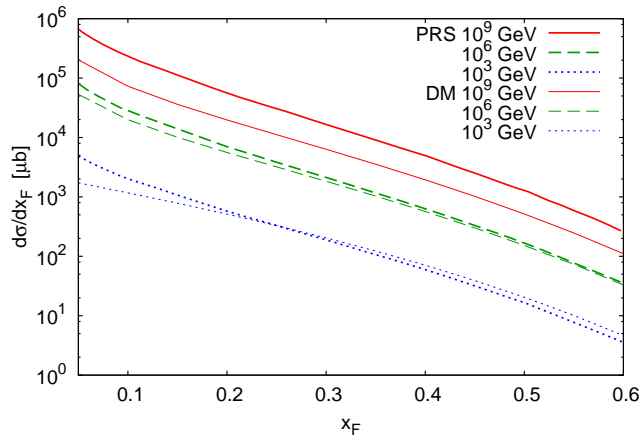


FIG. 4: The NLO QCD $pA \rightarrow c\bar{c}X$ differential cross section as a function of Feynman x_F for PRS [14] compared to the dipole model (DM) result for incident proton energies of 10^3 , 10^6 , 10^9 GeV. The thicker lines are PRS and the thinner lines with the same color are DM at the same energy.

III. CALCULATION OF NEUTRINO FLUXES

The lepton flux at sea level is calculated by solving the coupled set of differential equations that describes the cascade in the atmosphere initiated by the incident cosmic ray nucleons. We use the primary nucleon flux parametrization with a knee from Ref. [15]:

$$\phi_N(E) = \begin{cases} 1.7 E^{-2.7} & \text{for } E < 5 \cdot 10^6 \text{ GeV} \\ 174 E^{-3} & \text{for } E > 5 \cdot 10^6 \text{ GeV,} \end{cases} \quad (30)$$

where the cosmic ray energy E is given in GeV and the flux $\phi_N(E)$ in $\text{cm}^{-2} \text{s}^{-1} \text{sr}^{-1} (\text{GeV}/A)^{-1}$.

The cascade consists of production and attenuation through interactions and decay of the particles. We follow the analytic approximation method used in Refs. [14, 15, 62, 63] for calculating the flux. In Ref. [15] it was shown that this approximate solution agrees with a numerical Monte Carlo solution of the same equations.

The flux is calculated as a function of the slant depth X , which is a measure of the amount of atmosphere traversed by the particle. It is defined as the integral of the atmospheric density along its path through the atmosphere:

$$X(\ell, \theta) = \int_{\ell}^{\infty} d\ell' \rho(h(\ell', \theta)), \quad (31)$$

where $h(\ell, \theta)$ is the height at distance from the ground ℓ and zenith angle θ . A reasonable model for our purposes is an exponential atmosphere with [15]

$$\rho(h) = \rho_0 \exp(-h/h_0), \quad (32)$$

with $h_0 = 6.4$ km and $\rho_0 = 2.03 \times 10^{-3}$ g/cm³. The vertical depth of the atmosphere is $X \simeq 1300$ g/cm², while the horizontal depth is $X \simeq 36,000$ g/cm². We shall mostly be concerned with the vertical flux, $\theta = 0$, as the conventional flux is the smallest in the vertical direction. We will, however, show predictions for the flux in the horizontal direction as well.

The general form of the cascade equation for the flux $\phi_j = \phi_j(X, E)$ of particle species j at energy E and slant depth X is

$$\frac{d\phi_j}{dX} = -\frac{\phi_j}{\lambda_j} - \frac{\phi_j}{\lambda_j^{\text{dec}}} + \sum_k S(k \rightarrow j), \quad (33)$$

where λ_j is the interaction length, λ_j^{dec} is the decay length, and $S(k \rightarrow j)$ is the regeneration function, given by

$$S(k \rightarrow j) = \int_E^{\infty} dE' \frac{\phi_k(E')}{\lambda_k(E')} \frac{dn(k \rightarrow j; E', E)}{dE}. \quad (34)$$

For the case of production,

$$\frac{dn(k \rightarrow j; E_k, E_j)}{dE_j} = \frac{1}{\sigma_{kA}(E_k)} \frac{d\sigma(kA \rightarrow jY, E_k, E_j)}{dE_j} \quad (35)$$

is the distribution of secondary hadrons and σ_{kA} is the total inelastic cross section for kA collisions. For the case of decays,

$$\frac{dn(k \rightarrow j; E_k, E_j)}{dE_j} = \frac{1}{\Gamma_k} \frac{d\Gamma(k \rightarrow jY, E_j)}{dE_j}. \quad (36)$$

The nucleon, meson, and lepton fluxes are described by

the equations

$$\frac{d\phi_N}{dX} = -\frac{\phi_N}{\lambda_N} + S(NA \rightarrow NY) \quad (37)$$

$$\begin{aligned} \frac{d\phi_M}{dX} &= S(NA \rightarrow MY) - \frac{\phi_M}{\rho d_M(E)} \\ &\quad - \frac{\phi_M}{\lambda_M} + S(MA \rightarrow MY) \end{aligned} \quad (38)$$

$$\frac{d\phi_\ell}{dX} = \sum_M S(M \rightarrow \ell Y) \quad (39)$$

where $\ell = \mu, \nu_\mu, \nu_e$ and the mesons include unstable baryons: for prompt fluxes from charm $M = D^\pm, D^0, \bar{D}^0, D_s^\pm, \Lambda_c^\pm$. In Eq. (38) $d_M = c\beta\gamma\tau$ is the decay length.

The analytic solution relies on the approximate factorization of the fluxes into energy- and X -dependent parts. For the meson flux:

$$\frac{d\phi_M}{dX} = -\frac{\phi_M}{\rho d_M} - \frac{\phi_M}{\lambda_M} + Z_{MM} \frac{\phi_M}{\lambda_M} + Z_{NM} \frac{\phi_N}{\lambda_N} \quad (40)$$

with

$$Z_{kh} = \int_E^\infty dE' \frac{\phi_k(E', X, \theta)}{\phi_k(E, X, \theta)} \frac{\lambda_k(E)}{\lambda_k(E')} \frac{dn(kA \rightarrow hY; E', E)}{dE}. \quad (41)$$

We now make the standard assumption that $\phi_k(E, X, \theta) = E^{-\beta_k} \phi_k(X, \theta)$, so that if the energy spectrum falls as $E^{-\gamma-1}$, we have

$$Z_{kh} = \int_E^\infty dE' \left(\frac{E'}{E}\right)^{-\gamma-1} \frac{\lambda_k(E)}{\lambda_k(E')} \frac{dn(kA \rightarrow hY; E', E)}{dE}. \quad (42)$$

Eq. (37) for the nucleon flux then has the solution

$$\phi_N(X, E) = \phi(E) e^{-X/\Lambda_N(E)}, \quad (43)$$

where $\phi(E) \equiv \phi(0, E)$ is the primary flux of nucleons on the atmosphere and $\Lambda_N(E)$ is the nucleon attenuation length, defined as

$$\Lambda_N(E) = \frac{\lambda_N(E)}{1 - Z_{NN}(E)}, \quad (44)$$

where $\lambda_N(E)$ is the interaction length of nucleons in the atmosphere. It is given by

$$\lambda_N(E) = \frac{A}{N_0 \sigma_{pA}(E)}, \quad (45)$$

where $A = 14.5$ is the average atomic number of air, N_0 is Avogadro's number, and σ_{pA} is the total nucleon-air cross section. We take the parametrization from [64] for this cross section, and the Monte Carlo result from [15] for $Z_{NN}(E)$.

The meson fluxes are expressed in terms of the nucleon flux by solving the cascade equations separately at low and high energies, where the interaction and regeneration terms and the decay terms, respectively, can be

neglected. For the high energy flux we need the attenuation lengths of charmed hadrons in the atmosphere, which we replace by the corresponding quantities for K -mesons. These are approximated by

$$\Lambda_M(E) = \frac{A}{N_0 \sigma_{pA}(E)} \frac{\sigma_{pp}(E)}{\sigma_{Kp}(E)} \frac{1}{1 - Z_{KK}(E)}. \quad (46)$$

As for nucleons, we take Z_{KK} from [15] and σ_{pA} from [64]. The cross sections σ_{pp} and σ_{Kp} are taken from [55].

The final step is to obtain the lepton fluxes at high and low energies from Eq. (39) and the obtained meson fluxes, and interpolating between them for intermediate energy. This calculation is done in the limit $X \rightarrow \infty$. The Z -moments for the three-body decay modes $M \rightarrow \ell Y$ are calculated using expressions in Refs. [63, 64], and the lepton flux at intermediate energies is obtained by interpolating between the high- and low-energy solutions. In each of these regimes the meson fluxes are described by power laws $\phi_M(E) \propto E^{-\beta}$ where $\beta = \gamma$ in the low-energy regime and $\beta = \gamma + 1$ in the high energy regime, and γ is the index of the primary nucleon flux. The higher power of energy in the high energy flux is due to the appearance of the gamma factor in the decay length in the denominator of the meson flux.

The equations for the lepton fluxes then give

$$\phi_\ell^{\text{low}} = Z_{M\ell, \gamma+1} \frac{Z_{NM}}{1 - Z_{NN}} \phi_N(E) \quad (47)$$

$$\phi_\ell^{\text{high}} = Z_{M\ell, \gamma+2} \frac{Z_{NM}}{1 - Z_{NN}} \frac{\ln(\Lambda_M/\Lambda_N)}{1 - \Lambda_N/\Lambda_M} \frac{\epsilon_M}{E} \phi_N(E), \quad (48)$$

where ϵ_M , the critical energy for meson M , separates the low- and high-energy regions, where attenuation is dominated by decay and interaction. It depends on zenith angle, and is for the specific model of the atmosphere we use given by

$$\epsilon_M(\theta) = \frac{m_M c^2 h_0}{c\tau_M} f(\theta), \quad (49)$$

where $h_0 = 6.4$ km is a scale parameter for the isothermal height dependence of the atmospheric density [15]. For relatively small angles, $f(\theta) = 1/\cos\theta$, but for angles near horizontal, the angular dependence is more complicated. To compute the horizontal flux, we follow the approach of Ref. [63], leading to the replacement $\theta = 90^\circ \rightarrow \theta^* = 84.45^\circ$.

Further details of this procedure to solve the cascade equations semi-analytically are given, e.g., in Refs. [14, 15]. Our treatment here adds the fragmentation of the charm quarks into charmed hadrons, meaning that we must compute separately the moments Z_{ph} for each hadron M , including fragmentation functions in the calculation of the cross section. When fragmentation is neglected, we have the simple relation $Z_{ph} = f_h Z_{pc}$, where f_h is the fragmentation fraction.

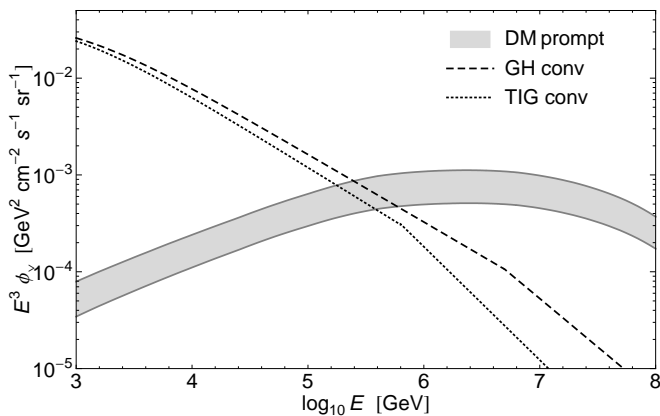


FIG. 5: Prompt and conventional $\nu_\mu + \bar{\nu}_\mu$ fluxes in the vertical direction. The shaded band is the theoretical uncertainty band for the prompt flux calculated in this paper with the dipole model. The dashed line shows the conventional flux from Gaisser and Honda (GH) [11] and the dotted line is the conventional flux calculated in Ref. [15] (TIG).

IV. RESULTS AND DISCUSSION

Our result for the vertical muon neutrino plus antineutrino flux from atmospheric charm is shown in Figure 5, which shows the theoretical uncertainty band for the DM calculation, estimated as described above. For comparison the conventional neutrino fluxes [11, 15] from π - and K -decays are also shown. We find that the vertical prompt muon neutrino flux becomes dominant over the conventional neutrino flux at energies between 10^5 GeV and $10^{5.5}$ GeV.

The theoretical uncertainty due to choices of gluon distribution, charm quark mass, factorization scale, and other parameters in the dipole model result in the range of fluxes represented by the shaded area in Figure 5. The shape of the prompt neutrinos is only weakly dependent on the choice of parameters, but the overall normalization could vary by up to a factor of two in this model for charm production.

We compare our result to three earlier calculations of the prompt neutrino flux:

1. Thunman, Ingelman and Gondolo (TIG) [15]. This was the first perturbative QCD calculation and was done at the leading order (LO) in α_s . It takes the fragmentation of charm quarks into account through Monte Carlo simulation using the Lund string model [65] implemented in the event generator Pythia [66]. The small- x PDFs are extrapolated with e.g., $xG(x, \mu^2) \sim x^{-0.08}$.
2. Pasquali, Reno and Sarcevic (PRS) [14]. This result uses the next-to-leading order (NLO) QCD result of [67] with power law extrapolations of the small- x PDFs. The PRS evaluation does not take fragmentation into account. We have therefore car-

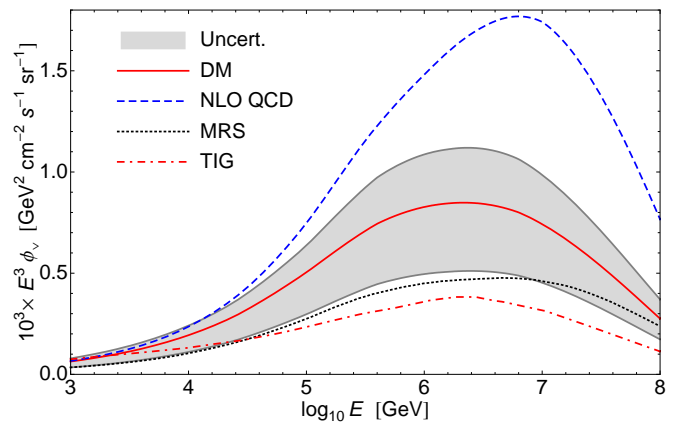


FIG. 6: Prompt muon neutrino fluxes obtained in perturbative QCD. The shaded area represents the theoretical uncertainty in the prompt neutrino flux evaluated in this paper, and the solid line in the band is our standard result. The dashed curve is the NLO perturbative QCD calculation of Ref. [14] (PRS), modified here to include fragmentation, the dotted curve is the saturation model result of Ref. [16] (MRS), and the dash-dotted curve is the LO perturbative QCD calculation of Ref. [15] (TIG).

ried out a simplified version of this calculation, taking fragmentation into account in the same way as we did for the DM calculation: we compute the charmed hadron cross section in leading order QCD using KK fragmentation functions [57], and multiply with a K-factor $K = \sigma(NLO)/\sigma(LO) \approx 2$. This reproduces the full NLO calculation of Ref. [14] at the parton level to an adequate accuracy.

3. Martin, Ryskin and Staśto (MRS) [16]. This calculation takes fragmentation into account by assigning the neutrino a fixed fraction of the momentum of the mother meson, and is done using the saturation model of Golec-Biernat and Wüsthoff [33] described above.

We show the results from these other evaluations of the vertical muon neutrino plus antineutrino flux together with our uncertainty band in Figure 6. The theoretical uncertainties in the standard NLO QCD calculation of the charm cross section are the choice of the renormalization and factorization scales, the charm mass, and the small x behavior of the gluon distribution [58]. The impact of some of these uncertainties on the neutrino flux has been studied in Ref. [17].

The MRS curve in Fig. 6 is at the lower border of our DM uncertainty band. There is approximately a factor of two between the MRS and the central DM results, coming from the different parameterizations of σ_d . The enhancement is also seen in calculations of photoproduction of heavy quarks [59] comparing the GBW model and the improved DM model of Eq. 13. The DM cross section for charm pair production in pp collisions lies within

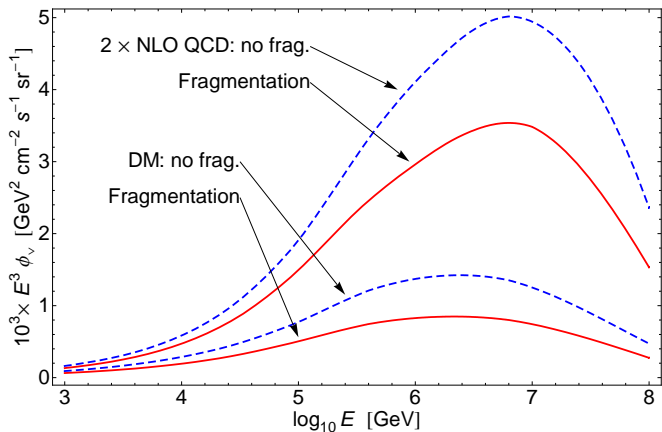


FIG. 7: The effect of fragmentation on predicted $\nu_\mu + \bar{\nu}_\mu$ fluxes. The solid lines are DM and NLO QCD (the latter multiplied by two to separate the lines) with Kniehl–Kramer fragmentation. The dashed lines are without fragmentation.

the uncertainty band of Ref. [58].

The effect of quark fragmentation on the neutrino fluxes is rather large because fragmentation reduces the energy of the charmed hadrons. For a given hadron energy, fragmentation effects require higher energy cosmic rays in the steeply falling cosmic ray flux. In Figure 7 we show the effect of including the KK fragmentation functions on both the NLO QCD and DM results. The NLO results are multiplied by a factor of two so that they can be distinguished easily from the DM results. The fragmentation reduces the flux by between 60% and 70%, and thus it is an important effect to take into account. The Peterson fragmentation function results differ by approximately 10% from the results shown in Figure 7. We include the uncertainty in fragmentation model in our estimate of the theoretical uncertainty; however, we do not consider the result without fragmentation in our uncertainty estimate.

Other perturbative QCD calculations are unlikely to give a much larger prompt neutrino flux than our upper limit, if saturation is indeed important. The theoretical expectation is that saturation is important at scales comparable to $\mu \sim m_c$ for small x values. If it would turn out that saturation *does not* occur at the relevant energy scales, the flux is still not expected to be much larger than the PRS result. In Figure 8, we therefore show a comparison of the uncertainty (blue, dark band) compared to the proposed uncertainty range from Ref. [6] (magenta, light band). In this plot we take the NLO QCD result as the upper theoretical limit. This gives a larger upper limit than in the earlier plots, which show only the uncertainty in the dipole model result. We stress that, since saturation is expected to be important on theoretical grounds, the uncertainty band in Figure 5 is our main result.

In order to obtain a flux as large as the upper line

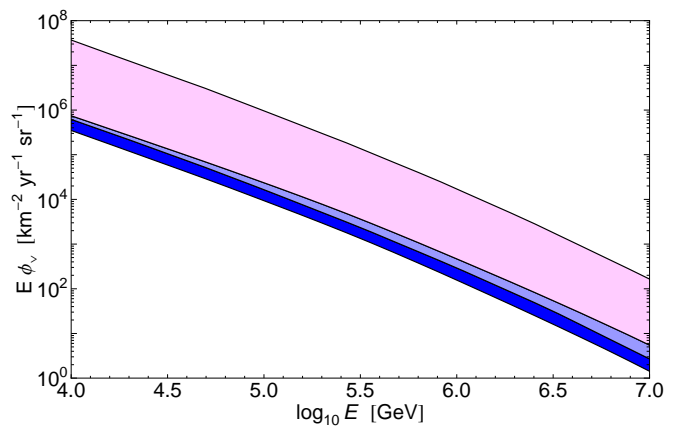


FIG. 8: Theoretical uncertainty band (blue, dark band), compared to the uncertainty band from Ref. [6] (magenta, light band) with the overlapping region shown as the middle (light blue) band. The flux is scaled by E , in units of $1/\text{km}^2\text{yr sr}$.

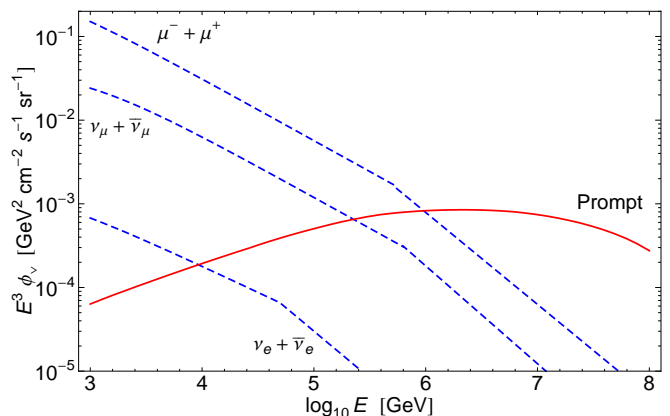


FIG. 9: Prompt (solid line) and conventional (dashed lines) fluxes of $\nu_\mu + \bar{\nu}_\mu$, $\nu_e + \bar{\nu}_e$, and $\mu^+ + \mu^-$. The conventional fluxes are from Ref. [15]. The three prompt fluxes are approximately equal and are therefore here represented by the $\nu_\mu + \bar{\nu}_\mu$ flux.

in the uncertainty band of Figure 8, we must multiply the upper uncertainty line of our DM result by a factor of 50. A cross section a factor of 50 times larger than the DM evaluation in proton-proton scattering would be incompatible with existing cross section measurements, as illustrated for example by Figure 6 of Ref. [31], which compares the DM result for charm production to fixed-target experimental data.

Measurable stau production rates from prompt atmospheric neutrinos as proposed in Ref. [6] would require the highest fluxes in the lighter band. Our evaluation of the prompt neutrino flux indicates that the upper limit of Ref. [6] is unrealistically large. The prompt neutrino flux is unlikely to be large enough for studying stau production from neutrino interactions with Earth and the subsequent detection in neutrino telescopes.

The flavor decomposition of an atmospheric neutrino

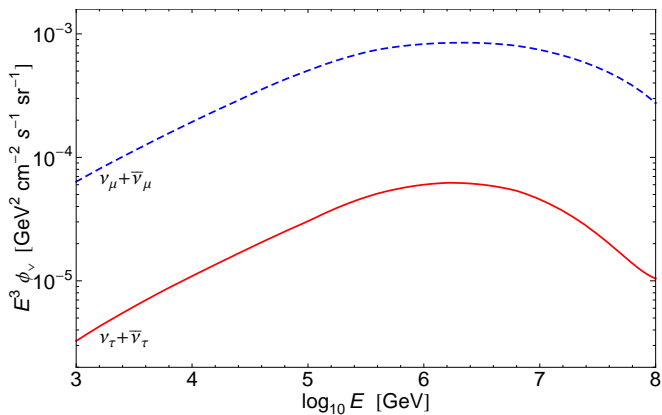


FIG. 10: Prompt $\nu_\tau + \bar{\nu}_\tau$ flux (solid line) compared with the prompt $\nu_\mu + \bar{\nu}_\mu$ flux (dashed line).

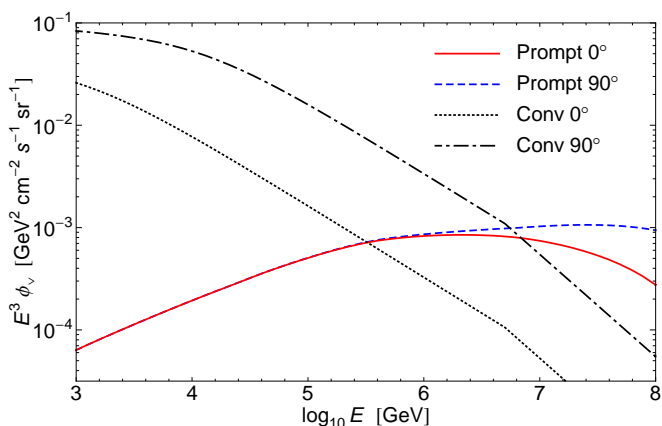


FIG. 11: Dependence on zenith angle of prompt and conventional $\nu_\mu + \bar{\nu}_\mu$ fluxes. The solid and dashed lines are DM with fragmentation in the vertical and horizontal directions, respectively. The dotted and dash-dotted lines are the Gaisser-Honda conventional fluxes [11] in the vertical and horizontal directions.

signal may be an interesting way to explore the prompt contribution. The prompt neutrino fluxes of $\nu_\mu + \bar{\nu}_\mu$ and $\nu_e + \bar{\nu}_e$ are identical, since the charmed mesons decay equally likely into electrons or muons. The prompt $\mu^+ + \mu^-$ flux is approximately equal to the neutrino fluxes. However, this does not hold for the conventional fluxes. Charged pions decay almost exclusively into muons, so the muon neutrino and muon fluxes are much larger than the electron neutrino flux. We show the $\nu_\mu + \bar{\nu}_\mu$ prompt flux together with the corresponding ver-

tical conventional fluxes of muons, muon neutrinos and electron neutrinos (and their antiparticles) in Figure 9. If experiments would be able to measure electron neutrino fluxes, the prompt flux will start dominating over the conventional flux for much lower energy $\sim 10^4$ GeV than for the muon neutrino or muon fluxes.

We note that the prompt flux of $\nu_\tau + \bar{\nu}_\tau$ from charm decays is much smaller than the other neutrino flavors [68], since only the D_s meson decays into ν_τ . The $\nu_\tau + \bar{\nu}_\tau$ flux from D_s decays is shown in Figure 10 together with the prompt $\nu_\mu + \bar{\nu}_\mu$ flux. We have not included the contribution from B -meson decays which could give a contribution on the order of 10–20% [16] since B -meson decays to ν_τ plus tau are kinematically allowed.

The vertical direction is the optimal direction for studying the prompt fluxes. In Figure 11 we show the prompt and conventional $\nu_\mu + \bar{\nu}_\mu$ fluxes in the vertical and horizontal directions. In the horizontal direction the prompt flux does not become larger than the conventional flux until very large energies $\sim 10^7$ GeV, where the actual number of neutrinos is quite low.

In summary, we have computed prompt neutrino and muon fluxes from cosmic ray interactions in the atmosphere that produce charm pairs. Our evaluation of the fluxes takes parton saturation effects into account via the dipole model, a model with a parametric form guided by QCD and constrained by data. We find that saturation effects in the dipole model decrease the prompt fluxes above 10^5 GeV. Our estimate of the theoretical uncertainty in the predicted fluxes in the dipole model is on the order of a factor of two. In comparison to other QCD or dipole model evaluations of the prompt flux, the range of predictions is approximately a factor of 6. Future measurements of the high energy neutrino flux will provide interesting constraints on QCD-based evaluations of the prompt flux of neutrinos, however, the prompt neutrino flux is unlikely to be large enough to probe non-standard model interactions.

Acknowledgments

We would like to thank Julia Becker, Magno Machado and Teresa Montaruli for helpful discussions. We are also grateful to Magno Machado for providing us with details of the results of [31]. The Feynman diagrams in Figures 1 and 2 where drawn using JaxoDraw [69]. This research was supported in part by US Department of Energy contracts DE-FG02-91ER40664, DE-FG02-04ER41319 and DE-FG02-04ER41298.

[1] J. Hosaka *et al.* [Super-Kamiokande Collaboration], Phys. Rev. D **74** (2006) 032002 [arXiv:hep-ex/0604011]; Y. Fukuda *et al.* [Super-Kamiokande Collaboration], Phys. Rev. Lett. **82** (1999) 2644 [arXiv:hep-ex/9812014].

[2] C. A. Currat [SNO Collaboration], Int. J. Mod. Phys. A **20** (2005) 3106.

[3] See, for example, V. S. Beresinsky and G. T. Zatsepin, Phys. Lett. B **28** (1969) 423; R. Engel, D. Seckel

- and T. Stanev, Phys. Rev. D **64** (2001) 093010 [arXiv:astro-ph/0101216]; L. A. Anchordoqui, H. Goldberg, D. Hooper, S. Sarkar and A. M. Taylor, Phys. Rev. D **76** (2007) 123008 [arXiv:0709.0734 [astro-ph]].
- [4] See, for example, J. G. Learned and K. Mannheim, Ann. Rev. Nucl. Part. Sci. **50** (2000) 679.
- [5] See, e.g., T. Han and D. Hooper, New J. Phys. **6**, 150 (2004); L. Anchordoqui, T. Han, D. Hooper and S. Sarkar, Astropart. Phys. **25**, 14 (2006); M. Kowalski, A. Ringwald and H. Tu, Phys. Lett. B **529**, 1 (2002); S. I. Dutta, M. H. Reno and I. Sarcevic, Phys. Rev. D **66**, 033002 (2002).
- [6] S. Ando, J. F. Beacom, S. Profumo and D. Rainwater, JCAP **0804** (2008) 029 [arXiv:0711.2908 [hep-ph]].
- [7] X. Bai [IceCube Collaboration], Nucl. Phys. Proc. Suppl. **175-176** (2008) 415.
- [8] V. Agrawal, T. K. Gaisser, P. Lipari and T. Stanev, Phys. Rev. D **53**, 1314 (1996) [arXiv:hep-ph/9509423].
- [9] G. Battistoni, A. Ferrari, P. Lipari, T. Montaruli, P. R. Sala and T. Rancati, Astropart. Phys. **12** (2000) 315 [arXiv:hep-ph/9907408].
- [10] M. Honda, T. Kajita, K. Kasahara and S. Midorikawa, Phys. Rev. D **52** (1995) 4985 [arXiv:hep-ph/9503439].
- [11] T. K. Gaisser and M. Honda, Ann. Rev. Nucl. Part. Sci. **52**, 153 (2002) [arXiv:hep-ph/0203272].
- [12] T. K. Gaisser and T. Stanev, Phys. Rev. D **57** (1998) 1977 [arXiv:astro-ph/9708146].
- [13] L. V. Volkova, Sov. J. Nucl. Phys. **31** (1980) 784 [Yad. Fiz. **31** (1980) 1510].
- [14] L. Pasquali, M. H. Reno and I. Sarcevic, Phys. Rev. D **59** (1999) 034020 [arXiv:hep-ph/9806428].
- [15] P. Gondolo, G. Ingelman and M. Thunman, Astropart. Phys. **5** (1996) 309 [arXiv:hep-ph/9505417].
- [16] A. D. Martin, M. G. Ryskin and A. M. Stasto, Acta Phys. Polon. B **34** (2003) 3273 [arXiv:hep-ph/0302140].
- [17] G. Gelmini, P. Gondolo and G. Varieschi, Phys. Rev. D **61**, 036005 (2000) [arXiv:hep-ph/9904457]; G. Gelmini, P. Gondolo and G. Varieschi, Phys. Rev. D **61** (2000) 056011 [arXiv:hep-ph/9905377].
- [18] G. Battistoni, C. Bloise, C. Forti, M. Greco, J. Ranft and A. Tanzini, Astropart. Phys. **4**, 351 (1996).
- [19] P. Berghaus, T. Montaruli and J. Ranft, arXiv:0712.3089 [hep-ex].
- [20] L. V. Gribov, E. M. Levin and M. G. Ryskin, Phys. Rept. **100** (1983) 1.
- [21] L. N. Lipatov, Sov. J. Nucl. Phys. **23**, 338 (1976); E. A. Kuraev, L. N. Lipatov and V. S. Fadin, Sov. Phys. JETP **44**, 443 (1976); **45**, 199 (1977); I. I. Balitsky and L. N. Lipatov, Sov. J. Nucl. Phys. **28**, 822 (1978).
- [22] G. Altarelli and G. Parisi, Nucl. Phys. B **126**, 298 (1977); V. N. Gribov and L. N. Lipatov, Yad. Fiz. **15**, 781 (1972) [Sov. J. Nucl. Phys. **15**, 438 (1972)]; Yu. L. Dokshitzer, Sov. Phys. JETP **46**, 641 (1977) [Zh. Eksp. Teor. Fiz. **73**, 1216 (1977)].
- [23] A. H. Mueller and J. w. Qiu, Nucl. Phys. B **268**, 427 (1986).
- [24] S. J. Brodsky and H. J. Lu, Phys. Rev. Lett. **64**, 1342 (1990).
- [25] S. J. Brodsky and A. H. Mueller, Phys. Lett. B **206**, 685 (1988); G. R. Farrar, L. L. Frankfurt, M. I. Strikman and H. Liu, Phys. Rev. Lett. **64**, 2996 (1990).
- [26] N. N. Nikolaev and B. G. Zakharov, Z. Phys. C **49**, 607 (1991).
- [27] B. Blaettel, G. Baym, L. L. Frankfurt and M. Strikman, Phys. Rev. Lett. **70**, 896 (1993); L. Frankfurt, A. Radyushkin and M. Strikman, Phys. Rev. D **55**, 98 (1997) [arXiv:hep-ph/9610274].
- [28] N. N. Nikolaev, G. Piller and B. G. Zakharov, Z. Phys. A **354**, 99 (1996) [arXiv:hep-ph/9511384].
- [29] J. Raufeisen and J. C. Peng, Phys. Rev. D **67**, 054008 (2003) [arXiv:hep-ph/0211422].
- [30] B. Z. Kopeliovich and A. V. Tarasov, Nucl. Phys. A **710**, 180 (2002) [arXiv:hep-ph/0205151].
- [31] V. P. Goncalves and M. V. T. Machado, JHEP **0704**, 028 (2007) [arXiv:hep-ph/0607125].
- [32] L. Motyka and N. Timneanu, Eur. Phys. J. C **27**, 73 (2003) [arXiv:hep-ph/0209029].
- [33] K. J. Golec-Biernat and M. Wüsthoff, Phys. Rev. D **59**, 014017 (1999) [arXiv:hep-ph/9807513].
- [34] J. Bartels, K. J. Golec-Biernat and H. Kowalski, Phys. Rev. D **66**, 014001 (2002) [arXiv:hep-ph/0203258].
- [35] A. H. Mueller, Nucl. Phys. B **415**, 373 (1994).
- [36] S. Munier, Proceedings of the RIKEN Theory Summer Program on RHIC physics, BNL-73263-2004, Brookhaven National Laboratory, July 2004; S. Munier, Nucl. Phys. A **755**, 622 (2005) [arXiv:hep-ph/0501149]; E. Iancu, A. H. Mueller and S. Munier, Phys. Lett. B **606**, 342 (2005) [arXiv:hep-ph/0410018].
- [37] R. Enberg, K. J. Golec-Biernat and S. Munier, Phys. Rev. D **72**, 074021 (2005) [arXiv:hep-ph/0505101].
- [38] L. D. McLerran and R. Venugopalan, Phys. Rev. D **49**, 2233 (1994) [arXiv:hep-ph/9309289]; Phys. Rev. D **49**, 3352 (1994) [arXiv:hep-ph/9311205]; Phys. Rev. D **50**, 2225 (1994) [arXiv:hep-ph/9402335].
- [39] J. Jalilian-Marian, A. Kovner, A. Leonidov and H. Weigert, Nucl. Phys. B **504**, 415 (1997) [arXiv:hep-ph/9701284]; Phys. Rev. D **59**, 014014 (1999) [arXiv:hep-ph/9706377]; H. Weigert, Nucl. Phys. A **703**, 823 (2002) [arXiv:hep-ph/0004044]; E. Iancu, A. Leonidov and L. D. McLerran, Phys. Lett. B **510**, 133 (2001) [arXiv:hep-ph/0102009]; E. Iancu, A. Leonidov and L. D. McLerran, Nucl. Phys. A **692**, 583 (2001) [arXiv:hep-ph/0011241]; E. Ferreira, E. Iancu, A. Leonidov and L. McLerran, Nucl. Phys. A **703**, 489 (2002) [arXiv:hep-ph/0109115].
- [40] I. Balitsky, Nucl. Phys. B **463**, 99 (1996) [arXiv:hep-ph/9509348]; Phys. Rev. Lett. **81**, 2024 (1998) [arXiv:hep-ph/9807434]; Phys. Rev. D **60**, 014020 (1999) [arXiv:hep-ph/9812311]; Phys. Lett. B **518**, 235 (2001) [arXiv:hep-ph/0105334].
- [41] F. Gelis, T. Lappi and R. Venugopalan, arXiv:0804.2630 [hep-ph].
- [42] Y. V. Kovchegov, Phys. Rev. D **60**, 034008 (1999) [arXiv:hep-ph/9901281].
- [43] E. Iancu, K. Itakura and S. Munier, Phys. Lett. B **590**, 199 (2004) [arXiv:hep-ph/0310338].
- [44] E. Levin and K. Tuchin, Nucl. Phys. B **573**, 833 (2000) [arXiv:hep-ph/9908317].
- [45] S. Munier, unpublished note at www.cpht.polytechnique.fr/cpht/munier/Notes/
- [46] G. Soyez, Phys. Lett. B **655**, 32 (2007) [arXiv:0705.3672 [hep-ph]].
- [47] A. H. Mueller and D. N. Triantafyllopoulos, Nucl. Phys. B **640**, 331 (2002) [arXiv:hep-ph/0205167]; D. N. Triantafyllopoulos, Nucl. Phys. B **648**, 293 (2003) [arXiv:hep-ph/0209121]; R. Enberg, Phys. Rev. D **75**, 014012 (2007) [arXiv:hep-ph/0612005].
- [48] S. Munier and R. Peschanski, Phys. Rev. Lett. **91**, 232001

- (2003) [arXiv:hep-ph/0309177]; Phys. Rev. D **69**, 034008
(2004) [arXiv:hep-ph/0310357]; Phys. Rev. D **70**, 077503
(2004) [arXiv:hep-ph/0401215].
- [49] N. Armesto, C. A. Salgado and U. A. Wiedemann, Phys. Rev. Lett. **94**, 022002 (2005) [arXiv:hep-ph/0407018].
- [50] H. Kowalski, T. Lappi and R. Venugopalan, Phys. Rev. Lett. **100**, 022303 (2008) [arXiv:0705.3047 [hep-ph]].
- [51] R. J. Glauber, in Lectures in Theoretical Physics, Vol. 1, Eds. W. E. Brittin and L. G. Duham (Interscience, New York, 1959).
- [52] V. N. Gribov, Sov. Phys. JETP **29**, 483 (1969) [Zh. Eksp. Teor. Fiz. **56**, 892 (1969)].
- [53] N. Armesto, Eur. Phys. J. C **26**, 35 (2002) [arXiv:hep-ph/0206017].
- [54] E. R. Cazaroto, F. Carvalho, V. P. Goncalves and F. S. Navarra, arXiv:0805.1255 [hep-ph].
- [55] W. M. Yao *et al.* [Particle Data Group], J. Phys. G **33**, 1 (2006).
- [56] C. Peterson, D. Schlatter, I. Schmitt and P. M. Zerwas, Phys. Rev. D **27**, 105 (1983).
- [57] B. A. Kniehl and G. Kramer, Phys. Rev. D **74**, 037502 (2006) [arXiv:hep-ph/0607306].
- [58] R. Vogt, Eur. Phys. J. ST **155**, 213 (2008) [arXiv:0709.2531 [hep-ph]].
- [59] V. P. Goncalves and M. V. T. Machado, Phys. Rev. D **71**, 014025 (2005) [arXiv:hep-ph/0410199].
- [60] A. D. Martin, R. G. Roberts, W. J. Stirling and R. S. Thorne, Phys. Lett. B **531** (2002) 216 [arXiv:hep-ph/0201127].
- [61] J. Pumplin, D. R. Stump, J. Huston, H. L. Lai, P. Nadolsky and W. K. Tung, JHEP **0207** (2002) 012 [arXiv:hep-ph/0201195].
- [62] T. K. Gaisser, *Cosmic rays and particle physics*, Cambridge University Press (1990).
- [63] P. Lipari, Astropart. Phys. **1** (1993) 195.
- [64] E. V. Bugaev, A. Misaki, V. A. Naumov, T. S. Sinegovskaya, S. I. Sinegovsky and N. Takahashi, Phys. Rev. D **58**, 054001 (1998) [arXiv:hep-ph/9803488].
- [65] B. Andersson, G. Gustafson, G. Ingelman and T. Sjöstrand, Phys. Rept. **97**, 31 (1983).
- [66] T. Sjöstrand, S. Mrenna and P. Skands, JHEP **0605**, 026 (2006) [arXiv:hep-ph/0603175].
- [67] M. L. Mangano, P. Nason and G. Ridolfi, Nucl. Phys. B **373**, 295 (1992); P. Nason, S. Dawson and R. K. Ellis, Nucl. Phys. B **303**, 607 (1988); P. Nason, S. Dawson and R. K. Ellis, Nucl. Phys. B **327**, 49 (1989) [Erratum-ibid. B **335**, 260 (1990)]; W. Beenakker, W. L. van Neerven, R. Meng, G. A. Schuler and J. Smith, Nucl. Phys. B **351**, 507 (1991); W. Beenakker, H. Kuijf, W. L. van Neerven and J. Smith, Phys. Rev. D **40**, 54 (1989).
- [68] L. Pasquali and M. H. Reno, Phys. Rev. D **59** (1999) 093003 [arXiv:hep-ph/9811268].
- [69] D. Binosi and L. Theussl, Comput. Phys. Commun. **161**, 76 (2004) [arXiv:hep-ph/0309015].